Connecting the Molecular Structure of Cutin to Ultrastructure and Physical Properties of the Cuticle in Petals of Arabidopsis[1][OPEN]

Sylwester Mazurek, Imène Garroum, Jean Daraspe, Damien De Bellis, Vilde Olsson, Antonio Mucciolo, Melinka A. Butenko, Bruno M. Humbel, and Christiane Nawrath*

University of Lausanne, Department of Plant Molecular Biology (S.M., I.G., C.N.) and Electron Microscopy Facility (J.D., D.D.B., A.M., B.M.H.), CH-1015 Lausanne, Switzerland; University of Wroclaw, Department of Chemistry, 50-383 Wroclaw, Poland (S.M.); and University of Oslo, Department of Biosciences, Section for Evolutionary Genetics, 0371 Oslo, Norway (V.O., M.A.B.)

ORCID IDs: 0000-0003-0750-7018 (M.A.B.); 0000-0003-1470-8459 (C.N.).

The plant cuticle is laid down at the cell wall surface of epidermal cells in a wide variety of structures, but the functional significance of this architectural diversity is not yet understood. Here, the structure-function relationship of the petal cuticle of Arabidopsis (*Arabidopsis thaliana*) was investigated. Applying Fourier transform infrared microspectroscopy, the cutin mutants *long-chain acyl-coenzyme A synthetase2* (*lacs2*), *permeable cuticle1 (pec1)*, *cyp77a6*, *glycerol-3-phosphate acyltransferase6* (*gpat6*), and *defective in cuticular ridges* (*dcr*) were grouped in three separate classes based on quantitative differences in the ν(C=O) and ν(C-H) band vibrations. These were associated mainly with the quantity of 10,16-dihydroxy hexadecanoic acid, a monomer of the cuticle polyester, cutin. These spectral features were linked to three different types of cuticle organization: a normal cuticle with nanoridges (*lacs2* and *pec1* mutants); a broad translucent cuticle (*cyp77a6* and *dcr* mutants); and an electron-opaque multilayered cuticle (*gpat6* mutant). The latter two types did not have typical nanoridges. Transmission electron microscopy revealed considerable variations in cuticle thickness in the *dcr* mutant. Different double mutant combinations showed that a low amount of C16 monomers in cutin leads to the appearance of an electron-translucent layer adjacent to the cuticle proper, which is independent of DCR action. We concluded that DCR is not only essential for incorporating 10,16-dihydroxy C16:0 into cutin but also plays a crucial role in the organization of the cuticle, independent of cutin composition. Further characterization of the mutant petals suggested that nanoridge formation and conical cell shape may contribute to the reduction of physical adhesion forces between petals and other floral organs during floral development.

Cuticle formation at the surface of epidermal cell walls was a crucial step in the evolution of land plants. This surface layer plays essential roles in plant development and physiology, creating a border between organs and an interface between the plant and its external biotic and abiotic environment. As a diffusion barrier, the cuticle regulates the flux of molecules entering and leaving the plant, including water, nutrients, agrochemicals, as well as diverse signaling molecules (Nawrath, 2006; Yeats and Rose, 2013). In addition, the cuticle imparts viscoelastic properties to the adjacent polysaccharide cell wall, thereby protecting the plant against mechanical damage (Bargel et al., 2006).

The ultrastructure of plant cuticles is highly diverse among different plant species as well as among different organs of the same species (Jeffree, 2006). Microscopic studies suggest the presence of a continuum between the inner polysaccharide cell wall and aliphatic polymers on the surface, giving rise to a more or less pronounced layered structure. The cuticle also is impregnated and covered with a complex mixture of soluble waxes. During plant development, the cuticle undergoes an organ-specific maturation process from a procuticle, which can expand during growth, to a complex mature cuticle, and this transition is accompanied by compositional alterations. The leaves and stems of Arabidopsis (*Arabidopsis thaliana*) have an electron-opaque reticulate cuticle, while the petals have an amorphous electron-lucent outer layer (sometimes

[1] This work was supported by the Swiss National Science Foundation (grant nos. 31003A_125009 and 31003A_146276 to C.N.), the Herbette Foundation (to C.N.), the Swiss Plant Science Web (to S.M.), and the Research Council of Norway (grant nos. 13785/F20 and 230849/F20 to V.O. and M.A.B.).

* Address correspondence to christiane.nawrath@unil.ch.

The author responsible for distribution of materials integral to the findings presented in this article in accordance with the policy described in the Instructions for Authors (www.plantphysiol.org) is: Christiane Nawrath (christiane.nawrath@unil.ch).

S.M. performed and evaluated FTIR experiments; I.G. generated genotypes and performed chemical analyses, including data evaluation; D.D.B., J.D., and A.M. performed electron microscopy studies; V.O. performed adhesion experiments and analysis of the data; B.M. H., M.A.B., and C.N. supervised research; C.N. conceived the project, complemented research, evaluated research data, and wrote the article with contributions of all the authors.

[OPEN] Articles can be viewed without a subscription.

www.plantphysiol.org/cgi/doi/10.1104/pp.16.01637

termed the cuticle proper) and a dark-staining fibrous cell wall zone, which may be referred to as the cuticle layer. Part of the latter also is assumed to contain cuticular lipids that fill the surface undulations called nanoridges (Nawrath et al., 2013). The structural and compositional characteristics of the cell wall-cuticle interface, and the factors that influence its architecture, have not been well characterized.

Cutin, an aliphatic polyester, is the prominent polymer of the cuticle in many species (Fich et al., 2016) and is usually characterized by the composition of its aliphatic monomers after chemical transesterification. Typical cutin monomers are 16- or 18-carbon fatty acids that have a hydroxy group at the ω-position and also midchain hydroxy or epoxy groups. Unsubstituted fatty acids, dicarboxylic acids (DCA), and glycerol, as well as low amounts of phenolic compounds, also are present (Kolattukudy, 2001). The cutin of Arabidopsis petals is rich in 10,16-dihydroxy C16:0 acid, a dominating constituent in many other plant species (Li-Beisson et al., 2013). Characterization of the cell wall-cuticle continuum also may be accomplished without depolymerization by spectroscopic methods, such as Fourier transform infrared spectroscopy (FTIR) and Raman spectroscopy (Heredia-Guerrero et al., 2014). The former has been used to assess the quantity of cutin in the petal cell wall-cuticle continuum of Arabidopsis (Mazurek et al., 2013); however, the relationship between polyester monomer composition and spectroscopic features remains to be determined.

The basic steps of the cutin biosynthetic pathway (i.e. precursor formation, export, and assembly) have been elucidated during the last decade, mainly by forward and reverse genetic approaches in Arabidopsis and tomato (*Solanum lycopersicum*; Beisson et al., 2012; Li-Beisson et al., 2013; Yeats and Rose, 2013). Briefly, CoA-activated hydroxy and epoxy fatty acids are synthesized through the concerted action of long-chain acyl-CoA synthetases (LACS) and cytochrome P450-dependent oxidases of the CYP86, CYP77, and CYP96 subfamilies (Bak et al., 2011). More specifically, a terminal hydroxy group is introduced by members of the CYP86 family, giving ω-hydroxy hexadecanoic acid (ω-OH C16:0), upon which CYP77A6 acts as a midchain hydroxylase forming 10,16-dihydroxy hexadecanoic acid (10,16-diOH C16:0; Li-Beisson et al., 2009). The hydroxylated fatty acids are then transferred to glycerol-3-phosphate by glycerol-3-phosphate acyltransferases (GPATs). GPAT enzymes involved in cutin biosynthesis have an additional phosphatase activity forming *sn*-2 monoacylglycerols as end products (Yang et al., 2010, 2012). The different members of the GPAT family have distinct substrate specificities; for example, GPAT6 is specific for the formation of *sn*-2 monoacylglycerols from C16 precursors and plays an important role in the formation of cutin in the floral organs of Arabidopsis (Li-Beisson et al., 2009) and of tomato fruit (Petit et al., 2016). Other types of molecules also may be precursors of cutin, since the acyltransferase of the BADH family DEFECTIVE IN CUTICULAR RIDGES (DCR) is required for the incorporation of 10,16-diOH C16:0 into cutin (Panikashvili et al., 2009). DCR has diacylglycerol acyltransferase activity and can form triacylglycerol molecules carrying 10,16-dihydroxy hexadecanoic acids in vitro (Rani et al., 2010), but the activity of DCR in vivo has not been established.

Although little is known about the mechanism of monomer export to the extracellular environment for polyester formation, it has been reported that different plasma membrane-localized ABC transporters of the ABCG family are required (Kretzschmar et al., 2011). The half transporters ABCG11 and ABCG13 affect the incorporation of all aliphatic cutin monomers (Bird et al., 2007; Luo et al., 2007; Panikashvili et al., 2010, 2011), while the full-size ABC transporter PEC1/ABCG32 affects only specific monomers, notably 10,16-diOH C16:0 and ω-OH C16:0 (Bessire et al., 2011; Fabre et al., 2016). Cutin synthases of the GDSL lipase family then perform the transesterification of the hydroxylated monomers to the growing polymer (Fich et al., 2016). Mono(10,16-diOH C16:0)-2-glycerol is a substrate of CUTIN SYNTHASE1 in tomato (Yeats et al., 2012). Nonenzymatic self-assembly of hydroxylated fatty acids into nanoparticles that was facilitated by pectin (homogalacturonans [HGs]) and nonenzymatic polymerization in vitro also have been reported (Heredia-Guerrero et al., 2008; Guzman-Puyol et al., 2015). Conceivably, such nonenzymatic processes also take place in vivo, such as during polymerization initiation (Heredia-Guerrero et al., 2008; Guzman-Puyol et al., 2015).

Little information exists regarding the structural organization of the mature polyester within the cuticle and the formation of the cell wall-cuticle continuum. However, studies of several cutin mutants have revealed characteristic changes in the morphology of the petal nanoridges (Panikashvili et al., 2010, 2011; Bessire et al., 2011; Shi et al., 2011), and mutants with a reduction of >95% of the amount of 10,16-dihydroxy hexadecanoic acid (*cyp77A6*, *gpat6*, and *dcr*) do not have petal nanoridges (Li-Beisson et al., 2009; Panikashvili et al., 2009). In addition, initial studies aimed at correlating the structure and function of cuticles, including an assessment of the physicochemical properties, have exploited micrometer-thick cuticles, such as those of tomato fruits (Heredia, 2003; López-Casado et al., 2007; Heredia-Guerrero et al., 2012; España et al., 2014).

Here, the relatively delicate cuticle of petals in Arabidopsis wild type and five cutin mutants was studied to identify the relationship between chemical monomer composition, spectroscopic features of cutin, and cuticle ultrastructure and physical properties. FTIR microspectroscopy and cuticle ultrastructure analyses were used to characterize Arabidopsis mutants that were divided into two groups based on the 10,16-dihydroxy-hexadecanoic acid content of their petals. Those with a substantial reduction could be further divided based on correlated changes in their ultrastructure and FTIR spectra. Additional structural defects in the *dcr* mutant petals, together with double mutant analysis, suggested

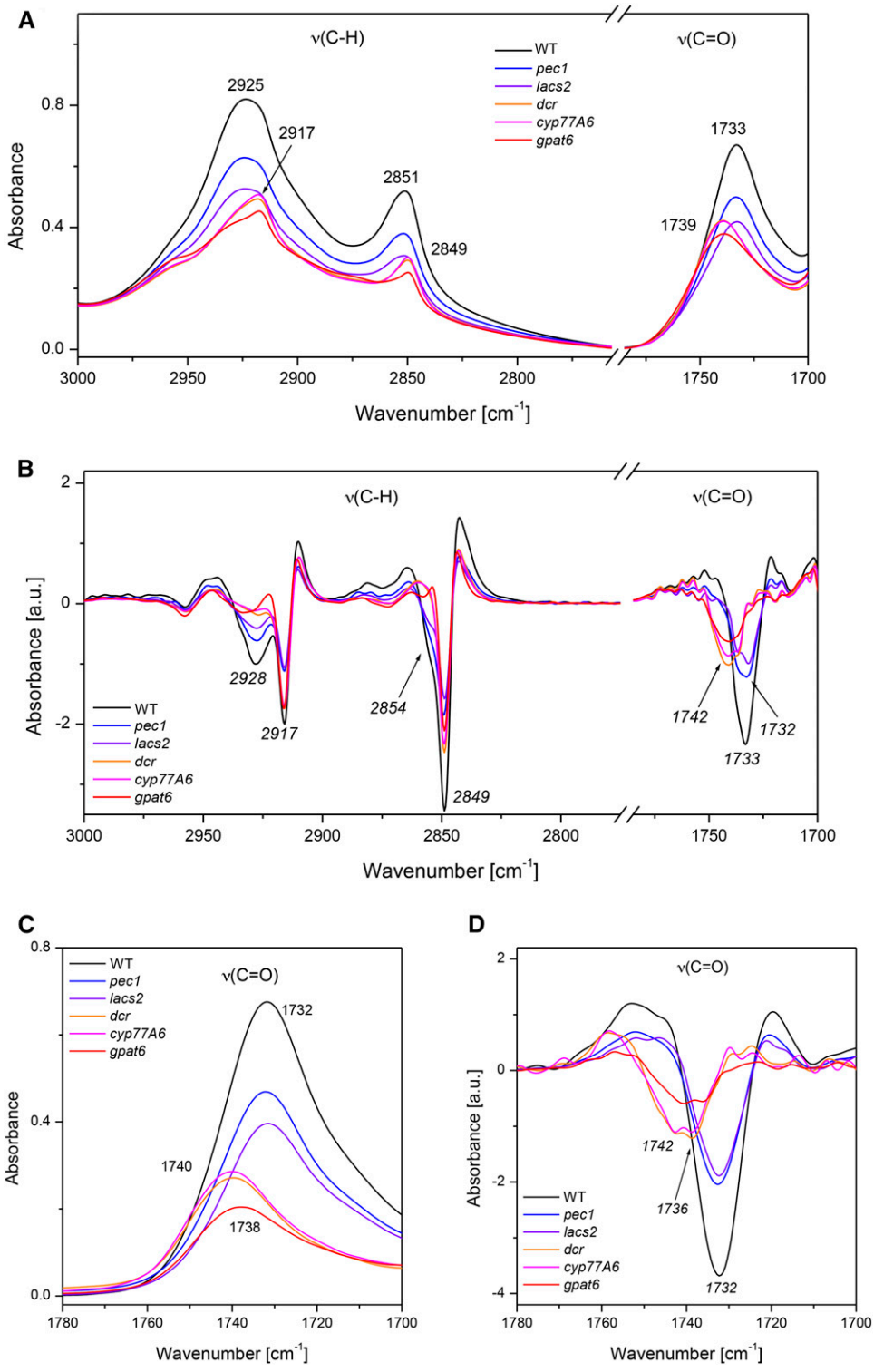

Figure 1. Spectral features of aliphatic polyesters in petals of different Arabidopsis genotypes. The spectral regions of the ν(C-H) and ν(C=O) band vibrations that are characteristic for aliphatic polyesters (A) and the corresponding second derivative (B) are depicted. A is an enlargement of the FTIR spectra showing the entire spectral range (Supplemental Fig. S1). Minima in B indicate the exact positions of dominant contributions building the complex peaks in the FTIR spectrotypes in A. The spectral regions of ν(C=O) band vibrations present in petals that had been digested by pectolyase and proteinase K (C) and its corresponding second derivative (D) are shown. Peak maxima are indicated by numbers and peak contributions by numbers in italics. WT, Wild type.

a key function of DCR in cuticle organization that is independent of cutin monomer composition and structure. The adhesion properties of petals on an artificial surface indicated that both cutin-dependent nanoridge formation and cell shape affect the physical surface properties of the petals.

RESULTS

FTIR Spectroscopy Distinguishes Different Classes of Petal Cutin Mutants in Arabidopsis

Characterization of petals of the *gpat6* mutant revealed not only a decrease of the intensity of the ν(C-H) and ν(C=O) band vibrations paralleling the reduced cutin amount (Fabre et al., 2016) but also a changed absorbance signal morphology associated with a specific shift of the position of the peak maxima compared with the wild type (Fig. 1; Supplemental Fig. S1). To identify the cause of the observed alterations, the Arabidopsis cutin mutants *lacs2*, *pec1*, *cyp77a6*, *gpat6*, and *dcr* (Bessire et al., 2007, 2011; Li-Beisson et al., 2009; Panikashvili et al., 2009) were investigated by transflection FTIR microspectroscopy. This technique is closely related to a previously established method (Mazurek et al., 2013). The only difference in transflection FITR is that the laser beam goes twice through the sample (Baker et al., 2014). When the infrared spectrotypes of the different mutants were calculated, *lacs2* and *pec1* showed variation only in the intensities of the ν(C-H) and ν(C=O) band vibrations (Mazurek et al., 2013; Fig. 1; Supplemental Fig. S2). The spectra of the *cyp77a6*, *dcr*, and *gpat6* mutants revealed narrower peaks of the asymmetric (ν_{asym}) and symmetric (ν_{sym}) stretching (C-H) band vibrations, with the maxima at 2,917 and 2,849 cm^{-1}, respectively (Fig. 1), instead of at 2,925 and 2,851 cm^{-1} observed for the wild type, *pec1*, and *lacs2* (Fig. 1). A distinct change of the ν(C=O) peak position to longer wavelengths also occurs. The ν(C=O) band vibrations were positioned at about 1,739 cm^{-1} in *gpat6*, *dcr*, and *cyp77a6* and at 1,733 cm^{-1} in the wild type, *pec1*, and *lacs2* (Fig. 1). The peak morphology of *gpat6*, however, was different from that of *cyp77a6* and *dcr*, placing *gpat6* in a separate group (Supplemental Fig. S2). Both the ν(C-H) and ν(C=O) vibrations were strongly diminished in the spectra of petals after acid depolymerization of polyesters, supporting the notion that these band vibrations derive from cutin. The observed residual peaks indicated contributions of the remaining cell wall polymers, such as methyl-esterified pectin, with a ν(C=O) band vibration at approximately 1,750 cm^{-1} (Supplemental Fig. S1; Mazurek et al., 2013).

The exact position of the peak maximum can be more accurately determined by calculating the second derivative of the spectrum. Differentiation of the spectrum results in the enhancement of the spectral resolution and can reveal hidden features that are not visible in raw data, improving the quality of the information gathered, especially from broad bands. The second derivative of the FTIR spectra of the wild type and the cutin mutants *lacs2* and *pec1* revealed the presence of two distinct contributions in the 2,900 to 2,975 cm^{-1} region of the ν_{asym}(C-H) band vibrations, namely at 2,917 and 2,928 cm^{-1}, whereas the *cyp77a6*, *dcr*, and *gpat6* mutants had only the former (Fig. 1). The same is true for the contributions at 2,849 and 2,855 cm^{-1} in the region of ν_{sym}(C-H) band vibrations, with only the former occurring in *cyp77a6*, *gpat6*, and *dcr*. The differentiation of the infrared spectra, furthermore, identified numerous contributions of ν(C=O) vibrations between 1,732 and 1,742 cm^{-1} that varied in the different genotypes (Fig. 1).

To obtain more accurate peak positions for aliphatic polyesters, petals were double digested with pectolyase and proteinase K to remove pectin as well as cell wall proteins. Although this treatment strongly reduced the signals in the 1,550 to 1,675 cm^{-1} and 1,000 to 1,200 cm^{-1} range of amides and polysaccharides, respectively, the band vibrations typical for aliphatic compounds and esters were only slightly influenced (Supplemental Fig. S3). Double digests clarified the peak contributions in the ν(C=O) range (Fig. 1; Supplemental Fig. S3), while the peaks in the ν(C-H) region were only minimally altered (Supplemental Fig. S3). Although the maximum of the ν(C=O) band vibrations of the wild type, *lacs2*, and *pec1* was at 1,732 cm^{-1}, the broadness and shape of the peaks indicated several contributions with slight variations in their ratios. In *cyp77a6* and *dcr*, the maximum position was at 1,740 cm^{-1}, and in *gpat6*, it was at 1,738 cm^{-1}, thus strongly different from the others. Calculating the second derivative of the spectra revealed that the differences in the peak maxima of *cyp77a6* and *dcr* versus *gpat6* have their origin in differences in the strength of contributions at 1,742 and 1,736 cm^{-1}.

In summary, three groups of infrared spectrotypes were identified based on peak positions of the characteristic ν(C=O) and ν(C-H) vibrations: (1) wild type/*lacs2*/*pec1*, (2) *cyp77a6*/*dcr*, and (3) *gpat6*, indicating qualitative changes in the aliphatic polyester. The shift in the peak positions in the ν(C-H) range could be associated with the absence of specific (C-H) vibrations in groups 2 and 3, pointing out the lack of certain types of aliphatic compounds in the cutin of the mutants. The shift of the peak position in the ν(C=O) range observed in groups 2 and 3 derived not only from the absence of the prominent ester band vibrations but also from new vibrations not present in group 1, suggesting the formation of different types of ester bonds in the *cyp77a6*/*dcr* and *gpat6* mutants.

Reduction in the Amounts in 10,16-Dihydroxy Hexadecanoic Acid Leads to Characteristic Changes in the Spectral Features of Petal Cutin

To explain the novel spectrotypes, the chemical composition of cutin monomers was investigated. Since FTIR measurements were performed on the blade of petals, the characterization of the same tissue for all the genotypes would be ideal. The *gpat6* and *dcr* mutants,

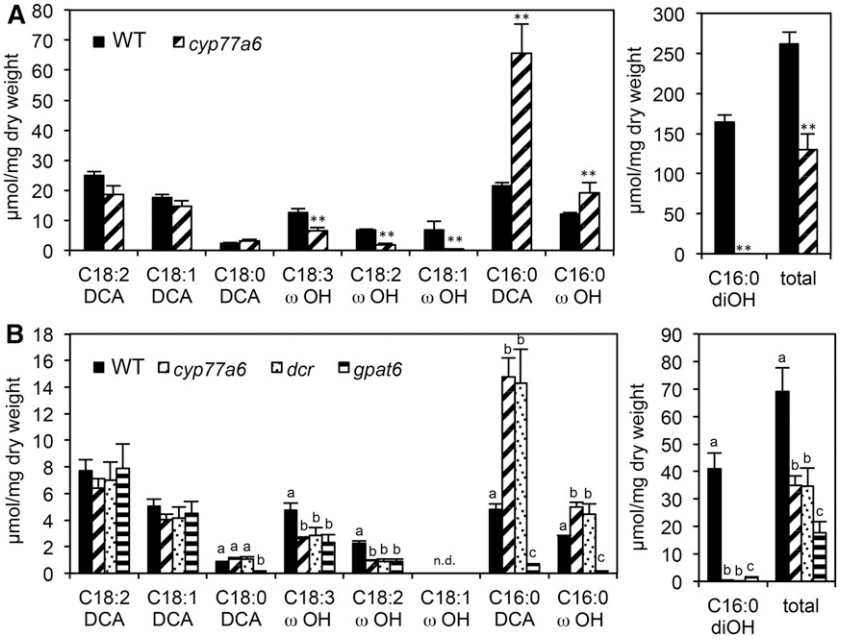

Figure 2. Cutin monomer composition of floral organs in different genotypes of Arabidopsis. Quantification of cutin monomers is shown in petal blades (A) and in entire flowers (B). Left graphs show the minor monomers, and right graphs show the major monomer 10,16-diOH C16:0 (C16:0 diOH) and the amount of all analyzed monomers (total). Asterisks denote significant differences as determined by Student's *t* test (**, $P < 0.01$). Different lowercase letters denote significant differences as determined by ANOVA and posthoc Tukey's HSD test at $P < 0.01$. WT, Wild type.

however, have developmental abnormalities leading to the formation of a strongly reduced number of flowers having well-formed petals, precluding such an analysis (Panikashvili et al., 2009; Fabre et al., 2016). The cutin monomer composition of petal blades was only characterized, therefore, for the wild type and *cyp77*a6, while that of entire flowers having well-formed petals was characterized for all mutants. As shown in Figure 2, the 10,16-dihydroxy hexadecanoate (10,16-diOH C16:0) was undetectable in *cyp77a6*, whereas the amounts of C16:0 DCA and ω-OH C16:0 were higher than in the wild type (300% and 60%, respectively) in both petal blades and entire flowers. The amounts of the monounsaturated, diunsaturated, and triunsaturated ω-OH C18 acids also were reduced in *cyp77a6*. Thus, the total amount of oxygenated fatty acids was approximately 50% lower in *cyp77a6* than in the wild type in both organs (Fig. 2).

The cutin composition of *cyp77a6* and the wild type was nearly identical in petal blades and entire flowers, despite the approximately four times higher amount of cutin in the former. Thus, a comparison of the composition of cutin of entire flowers of different genotypes with the respective spectrotypes measured on petal blades should be meaningful. Figure 2 shows that the cutin composition of *cyp77a6* and *dcr* was identical in entire flowers. All the oxygenated C16:0 monomers (i.e. C16:0 DCA, ω-OH C16:0, and 10,16-diOH C16:0) in *gpat6*, by contrast, were reduced, resulting in an overall reduction of 75% of cutin monomers compared with the wild type. A reduction of all oxygenated monomers in *lacs2* petals led to a 45% decrease in total cutin (Supplemental Fig. S4), while in *pec1* petals, the overall reduction in ω-oxygenated and midchain hydroxylated fatty acids was 30% and 40%, respectively (Bessire et al., 2011; Fabre et al., 2016).

In summary, cutin having a relatively equal reduction in both ω- and midchain oxygenated monomers of maximal 50% results in the same peak position of the ν(C-H) and ν(C=O) band vibrations in the infrared spectrum, namely at 2,925 and 2,851 as well as 1,733 cm^{-1}, respectively. Only the intensity of these vibrations changes according to the quantity of the polyester, as shown previously (Mazurek et al., 2013). The negligible amounts of 10,16-diOH C16:0 in the cutin of group 2 and 3 mutants correlated well with the missing peaks in the ν(C-H) region, indicating that the absence of midchain hydroxyl groups leads to peak absence. The novel band vibrations in the ν(C=O) region in spectra of these mutants potentially imply change(s) in a polyester lacking 10,16-diOH C16:0. Different amounts of other ω-oxygenated monomers in the cutin of these mutants might explain the minor differences between peak positions of the ν(C=O) bands at 1,740 and 1,738 cm^{-1} visible on spectra of petals after double digestion.

This notion was further investigated by characterizing cutin of expanded Arabidopsis wild-type leaves, which have a very low content in 10,16-diOH C16:0 (Fabre et al., 2016). FTIR spectra of epidermal tissue prepared from expanded leaves were characterized by the presence of very narrow peaks of the ν_{asym}(C-H) and ν_{sym}(C-H) vibrations at 2,915 and 2,848 cm^{-1}, respectively, similar to those of *cyp77a6* in petals at 2,917 and 2,849 cm^{-1} (Fig. 3). The ν(C=O) vibrations resulted in a broad peak that had a maximum at 1,737 cm^{-1} (Fig. 3). Thus, the cutin of the wild-type leaf epidermis has similar spectral features to the petal cutin of the *cyp77a6* mutant. These results further support the hypothesis that the differences in the ν(C-H) and ν(C=O) band vibrations characterizing group 2 and 3 cutin arise from the near absence of 10,16-diOH C16:0 and the resulting structural changes in the polyester.

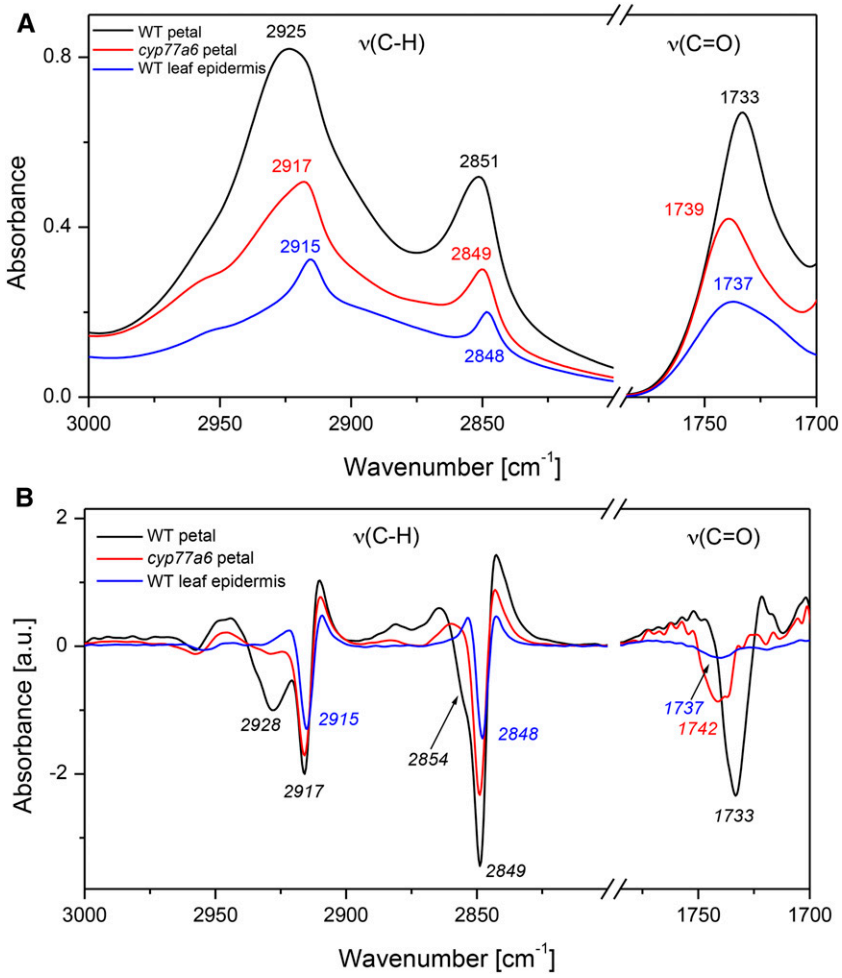

Figure 3. Spectral features of cutin in different organs of Arabidopsis. Fragments of FTIR spectra showing the regions of ν(C-H) and ν(C=O) band vibrations of petals and of leaf epidermis (A) and the corresponding second derivative of the spectra (B). Peak positions in the spectra are indicated by numbers. Spectral contributions revealed in the second derivative of the spectra are indicated in italics. WT, Wild type.

Nanoridges and Cell Shape Influence the Physical Surface Properties of Arabidopsis Petals

The preparation of petals from different genotypes for FTIR microscopy revealed high variation in their adhesion properties to glass plates and other microscope slides. Wild-type petals mounted on glass slides fail to adhere once dry, falling off the surface if perturbed, while petals of *cyp77a6*, *gpat6*, and *dcr* adhere so strongly that forcibly removing them leads to tissue tearing (Fig. 4). Adhering petals of *pec1* could be removed when applying a force to the petals without rending the tissue (Fig. 4). Petals of *lacs2*, however, had variable adhesion properties ranging from none to very strong, with tissue tearing resulting if removed (Fig. 4).

To quantify the force needed to break the contact between the petals and the glass slide, a load transducer was employed that had been constructed to measure the force needed to remove an Arabidopsis petal from the receptacle of the flower (Stenvik et al., 2008). In this study, the force needed to remove a single adhered petal from a whole flower by pulling on the remaining flower parts was measured. This force could be defined for *pec1*, *gpat6*, *dcr*, and *cyp77a6* petals. A force for petals that did not or only weakly adhered to the glass slides could not be quantified, which was true for 100% and 60% of the wild-type and *lacs2* petals, respectively. The lowest force that could be measured was 0.5-g equivalents; therefore, *lacs2* petals that were attached to the glass slides but fell off in the process of clamping needed a force of less than 0.5-g equivalents for removal. The measurable adhesion forces were lowest for *pec1*, whose petals could be detached from the glass slide without rending the petal tissue (Fig. 4), and highest for *cyp77a6*, while *gpat6* and *dcr* had intermediate values (Fig. 4).

Since surface morphology might influence adhesion properties, all the genotypes were investigated by cryoscanning electron microscopy. As reported earlier, *gpat6*, *dcr*, and *cyp77a6* lacked nanoridges correlating to the negligible amounts of 10,16-diOH C16:0 (Supplemental Fig. S5; Li-Beisson et al., 2009; Panikashvili et al., 2009). Cell shape on the adaxial side of the petal varied among the different genotypes; that is, *dcr* had more elongated cells than *cyp77a6* and *gpat6* (Supplemental Fig. S5). The petal epidermal cells of *pec1* and *lacs2* plants with reduced amounts of 10,16-diOH C16:0 differed in cell shape and surface morphology

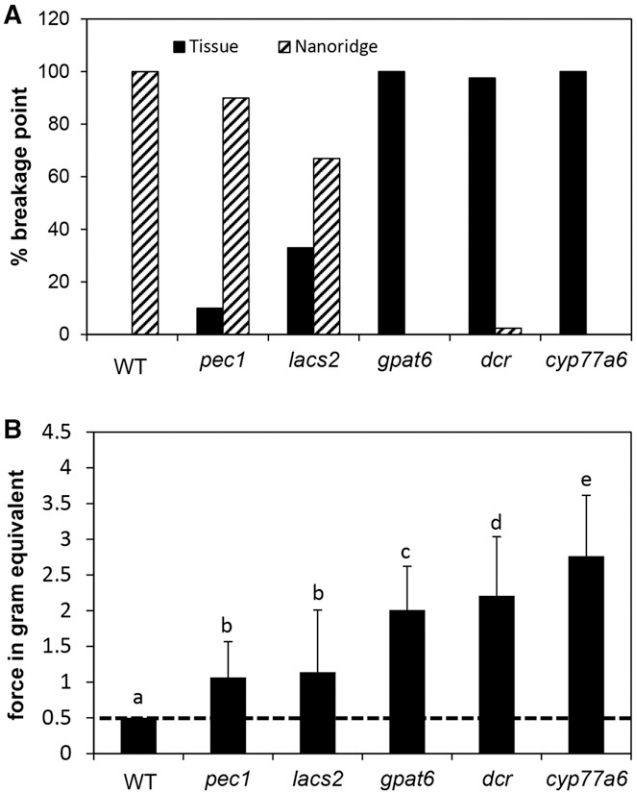

Figure 4. Adhesion and breakage point analysis of petals of different genotypes. A, The breakage point is given for petals that were adhering to a glass plate and were separated by force. Tissue indicates tissue disrupted, leaving the remaining petal on the glass slide, and Nanoridge indicates petal lifted off the glass slide without recognizable tissue damage. $n = 30$ to 80. B, The force was determined with which the petal-glass slide contact was broken. Samples that detached with a force lower than 0.5 g could not be handled (disrupted line). All wild-type (WT) samples and 60% of the *lacs2* samples were thus set to 0.5 g. Different letters indicate significant differences as determined by ANOVA/posthoc Tukey-Kramer test at $P < 0.05$.

(Supplemental Fig. S6). The *pec1* mutant had regular shallow nanoridges, with subtle differences in cell morphology, being slightly more roundish than in the wild type (Supplemental Fig. S6). The *lacs2* mutant cells had fewer nanoridges than *pec1*, correlating to a stronger reduction in cutin monomers (Supplemental Fig. S6). These few nanoridges were at the tips, leaving large parts of the surface smooth (Supplemental Fig. S6). The *lacs2* cells, moreover, were more pointed than those of *pec1* and the wild type (Supplemental Fig. S6).

Combining the above observations suggests that nanoridges reduce the contact surface between epidermal cells and glass slides. In other words, the smoother the cell surface, the greater the force needed to remove them from the glass slides. In *lacs2* plants, the reduction of nanoridges was partially compensated for by the presence of pointed cells. Presumably, their uneven distribution resulted in the wide range of adhesion observed. Other parameters possibly influencing the physical adhesion properties of petals to glass slides, such as the composition of the cutin, cannot be excluded.

The Ultrastructure of the Cuticle Reflects the Monomer Composition of Cutin

To evaluate the influence of cutin composition and the resulting macromolecular structures on the ultrastructure of the cuticle and the underlying cell wall, transmission electron microscopy (TEM) studies were performed. The cuticle ultrastructure of petals was investigated at the tip of the epidermal cells on the adaxial (Fig. 5) and abaxial sides (Supplemental Fig. S7) in cross sections that were perpendicular to the cell surface. Similar to previous reports (Bessire et al., 2007; Li-Beisson et al., 2009; Panikashvili et al., 2009), three morphologically distinct zones were present in the outer epidermal cell wall of the wild type. The innermost zone is the primary cell wall adjacent to but continuous with more electron-opaque regions that also are present in nanoridges (i.e. the so-called cuticle layer). The cuticle proper is external to the cell wall, forming a continuous layer of amorphous electron-translucent material covering the entire surface of the cell, including the nanoridges, and is sharply separated from the underlying cell wall layers (Fig. 5; Supplemental Fig. S7).

This structural organization of cell wall and cuticle as well as the appearance of the cuticle proper were not altered on either side of the petal in the *lacs2* mutant, although nanoridges were more irregularly shaped and sometimes shallower (Fig. 5; Supplemental Fig. S7). The cuticle proper and cell wall were similar in width in *lacs2* and the wild type, 100 and 150 nm, respectively (Supplemental Fig. S8). The structure of the cell wall-cuticle continuum, by contrast, was strongly altered in the *cyp77a6* mutant. Besides a lack of nanoridges, no sharp boundary between the cell wall and the cuticle was formed, and fibrous cell wall-like material was sometimes also seen within the otherwise amorphous cuticle proper. The cell wall was uniformly stained (i.e. a cuticular layer could not be distinguished), and the cuticle proper was very translucent (Fig. 5). The low degree of osmium staining of the cuticle proper might be explained by the higher proportion of saturated fatty acids in cutin, since osmium reacts preferentially with double bonds (Fig. 2; Hayat, 2000). In the absence of nanoridges, the cuticle proper was much thicker than in the wild type, ~300 and 260 nm thick on the adaxial and abaxial sides, respectively. The cell wall was likewise broader, measuring 220 and 180 nm on the adaxial and abaxial sides, respectively (Supplemental Fig. S8).

The appearances of the cuticle proper and cell wall-cuticle interface of the *dcr* mutant were similar to those of *cyp77a6* (Fig. 5; Supplemental Fig. S7). In both genotypes, a thin structurally distinct lamella was recognizable on the cuticle surface, designated the oCu. The presence of fibrous cell wall-like material within the cuticle proper, however, was more pronounced in *dcr* than in *cyp77a6*, in particular on the abaxial side, where cell wall material was dispersed within the entire cuticle proper of *dcr* (Fig. 5; Supplemental Fig S7). The

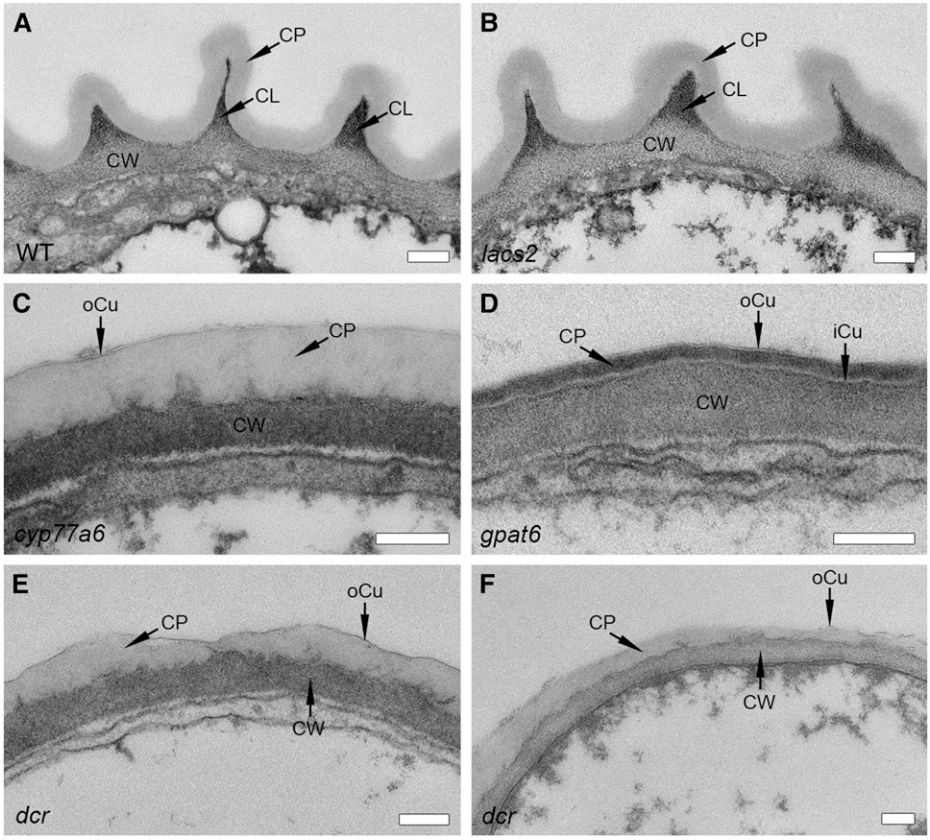

Figure 5. Cuticle ultrastructure of the adaxial side of petals in different genotypes of Arabidopsis. The cell wall-cuticle continuum of Arabidopsis petals embedded in Spurr's resin is pictured at the apex of the conical epidermal cell. CL, Cuticular layer; CP, cuticle proper; CW, cell wall; iCu, inner cuticle lamella; oCu, outer cuticle lamella; WT, Wild type. Bars = 200 nm.

thickness of the cuticle proper of the *dcr* mutant varied from 10 to 400 nm (Fig. 5), being more pronounced on the adaxial side, where width variations occurred in most epidermal cells, than on the abaxial side, where they were rare (Supplemental Fig. S9). These phenotypes indicate that DCR absence strongly affects cuticle organization, albeit in a slightly different manner on the two sides of the petal.

Although nanoridges are largely absent from *gpat6*, *cyp77a6*, and *dcr*, the wall ultrastructure of the *gpat6* mutants differs markedly (Fig. 5; Supplemental Fig. S7). Most striking was the separation of the cell wall and cuticle by a fine translucent layer at the interface, here named the iCu (Fig. 5; Supplemental Fig. S7). The principal layer of the cuticle proper was very uniform, being approximately 50 nm thick and more electron opaque than the cuticle proper of the wild type (Supplemental Fig. S8). The stronger staining with osmium of the cuticle proper correlated well with the higher proportion of unsaturated cutin monomers (Fig. 2; Hayat, 2000). Similar to *cyp77* and *dcr*, a very thin oCu was present toward the surface that was only identifiable when deposits were present on its surface (Fig. 5; Supplemental Fig. S7). The *gpat6* mutant had a cuticle with a highly lamellated structure, both on the adaxial and abaxial sides. Despite the low amount of cutin, a waving in the cell wall reminiscent of nanoridges was sometimes present that correlated to the very low but significant amount of 10,16-diOH C16:0 (Fig. 2).

In summary, *cyp77a6*, *gpat6*, and *dcr*, having very low to negligible amounts of 10,16-diOH C16:0, had a different organization of the cuticle-cell wall continuum, while *lacs2* had only a reduction in the number of nanoridges. Particularly unexpected were the variations in the thickness of the petal cuticle of the *dcr* mutant that were not present in the other group 2 mutant, *cyp77a6*, since neither FTIR nor compositional analyses had indicated any differences between these two genotypes.

Pectic HG Distribution Reflects Cuticle Ultrastructure

To better characterize the different cuticle structures, the cell wall-cuticle continuum was investigated by immunocytochemistry. The antibodies LM19 and LM20, against deesterified and esterified pectic HG, respectively (Verhertbruggen et al., 2009), were selected, as HG may be present in cell wall and the different cuticle layers (Jeffree, 2006; Guzman-Puyol et al., 2015; Segado et al., 2016). In the epidermal cells of wild-type petals, esterified HG is present in the outer epidermal cell wall, subjacent to the cuticle and thus also in nanoridges (Fig. 6; Supplemental Fig. S9). HG epitopes are typically absent from the cuticle proper, except sometimes at the base of nanoridges (Fig. 6; Supplemental Fig. S9).

Interestingly, in immunolabeled sections, the HG-rich zone of the cell wall was more electron opaque

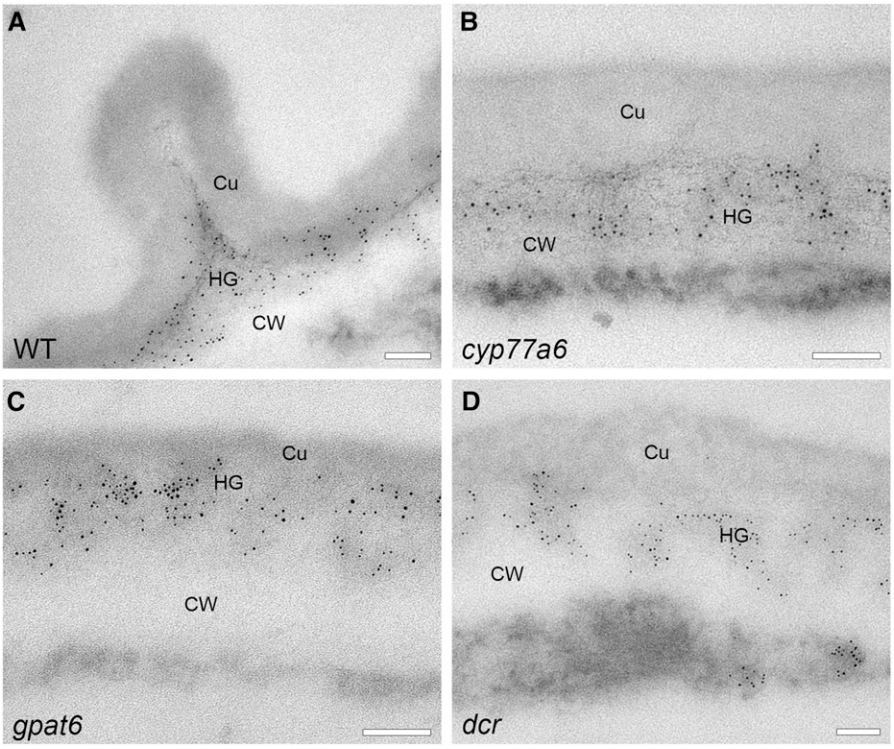

Figure 6. Localization of HG in the cell wall-cuticle continuum on the adaxial side of petals of different Arabidopsis genotypes. LM20 labeling shows esterified HG domains on sections embedded in LR White resin. The cell wall-cuticle continuum is depicted at the apex of the petal epidermal cell. Cu, Cuticle, CW, cell wall; WT, wild type. Bars = 100 nm.

and the nonlabeled zone was more electron translucent than in the sections prepared for structural analyses (Fig. 6). The cell wall also had a less fibrous appearance. The reversal, in contrast, may arise from the different fixation/embedding methods but also from the antibody labeling, because controls with the primary and secondary antibody alone resulted in weak modifications of the cell wall appearance (Supplemental Fig. S10). Immunolabeling of sections fixed and embedded in Spurr's resin showed the same localization of HG in the outer cell wall zone and within nanoridges, albeit with strongly reduced efficiency (Supplemental Fig. S10). This observation supports that the general cell wall structure had been maintained. Labeling with the LM19 antibody indicated that both esterified and deesterified pectic HG was present at similar positions in wild-type epidermal petal cells (Supplemental Fig. S10).

Since both LM19 and LM20 gave quasi-identical results in the outer cell wall and cuticle, only the labeling of esterified HG with LM20 is presented here. On the adaxial side of group 2 and 3 petals, LM20 label was present in the outer zone of the cell wall but not in the cuticle proper (Fig. 6). On the abaxial side of the group 2 petals, by contrast, a patchy labeling of the cuticle proper with the LM20 antibody was detected, indicating that the islands of fibrous cell wall material that had been observed within the cuticle proper of these genotypes contain HG and, potentially, also other polysaccharides (Supplemental Fig. S9). LM20 did not label the cuticle proper of the *gpat6* group 3 mutant (Fig. 6; Supplemental Fig. S9), indicating an absence of HG-rich polysaccharides. The HG immunochemistry studies thus support the conclusions based on an analysis of the ultrastructure of the cuticle employing sections embedded in Spurr's resin, despite less preservation of detail in LR White resin-embedded material, which is more suitable for immunochemistry.

DCR and GPAT6 Contribute Different Features to the Petal Cuticle

To differentiate the roles that DCR and GPAT6 play in structuring the cuticle, double mutant combinations were generated: *cyp77a6 dcr*, *cyp77a6 gpat6*, and *dcr gpat6*. These double mutants had stronger developmental abnormalities during flower formation, leading to a reduced number of well-formed petals in comparison with their parental lines. An analysis of the amount and composition of cutin performed on the *cyp77a6 gpat6* double mutant revealed a complete absence of 10,16-diOH C16:0 (Supplemental Fig. S4). Because of developmental defects, the same analysis of *cyp77a6 dcr* and *dcr gpat6* was not possible. FTIR analysis, however, indicated that cutin was more reduced in the double mutants than in their parents. A full spectral analysis of the polyester by FTIR also was not feasible because of low signal intensity and the low cutin-to-esterified pectin ratio.

The ultrastructure of the cell wall-cuticle continuum on both sides of petals of all three double mutants was investigated by TEM with sections prepared for analysis of ultrastructure and immunocytochemistry. Characterization of the cell wall-cuticle continuum of the *cyp77a6 gpat6* double mutant demonstrated that *gpat6* is epistatic to *cyp77a6*. Namely, the cuticle of the *cyp77a6 gpat6*

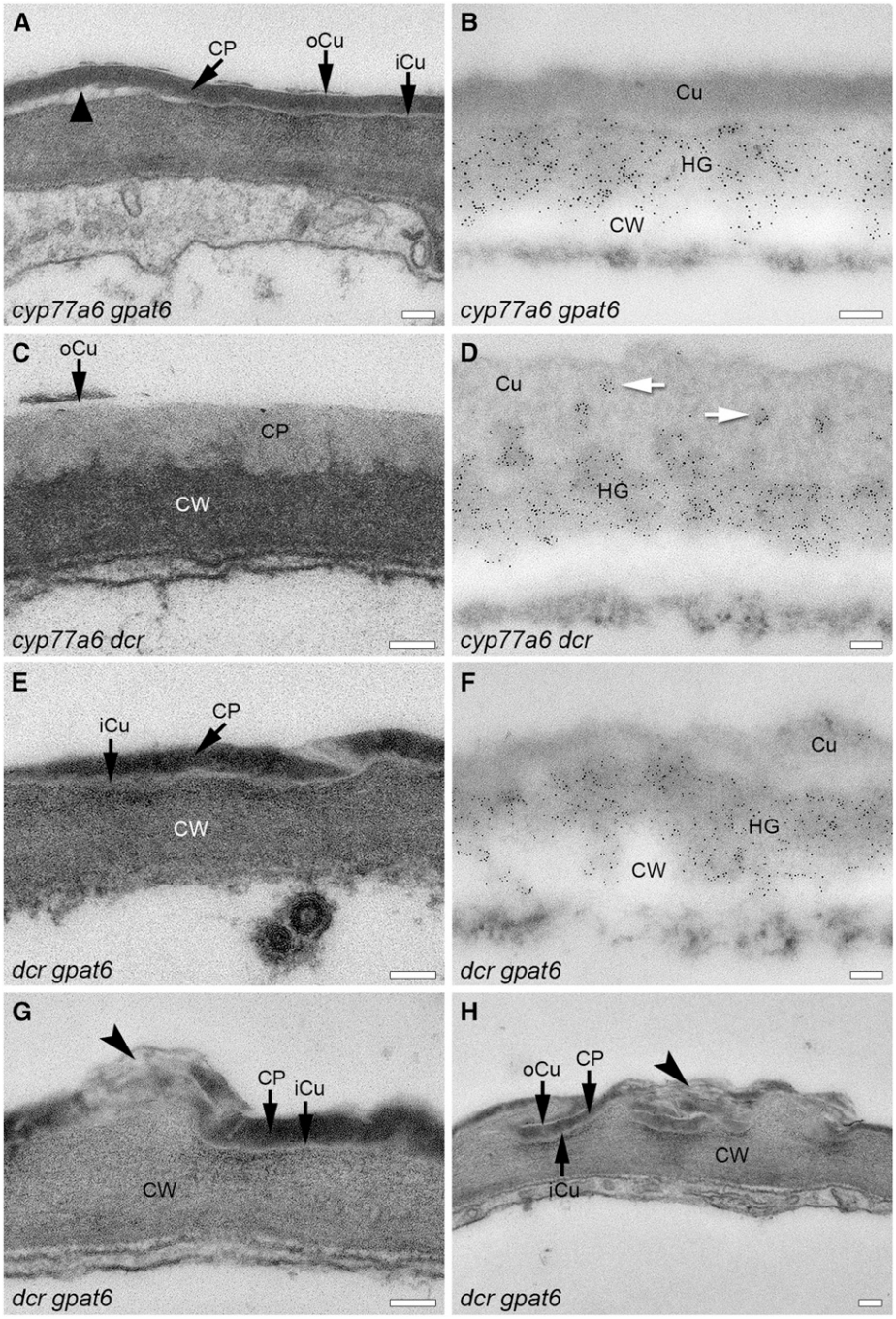

Figure 7. Ultrastructure of the cuticle and localization of HG in the cell wall-cuticle continuum in different double mutants having low amounts of 10,16-diOH C16:0. The cell wall-cuticle continuum on the abaxial side of the petal at the apex of the epidermal cells is shown. The ultrastructure of the cuticle is depicted in A, C, E, G, and H on sections that were embedded in Spurr's resin. LM20 labeling of esterified HG domains (HG) in the cell wall-cuticle continuum is shown in B, D, and F on sections embedded in LR White resin. CP, Cuticle proper; Cu, cuticle; CW, cell wall. White arrows indicate islands of dispersed HG-rich cell wall. Black arrowheads indicate areas with multilayered cuticles. The black triangle points to an area of decreased cuticular attachment. Bars = 100 nm.

double mutant was as thick as in *gpat6*, approximately 50 nm (Supplemental Fig. S8), and also was organized in several layers: the iCu, the cuticle proper, and sometimes also an oCu (Figs. 7 and 8). The cuticle was sometimes separated from the cell wall along the iCu, indicating a greater fragility of this layer in *cyp77a6 gpat6* (Fig. 7). That LM20 did not label the electron-lucent zone at the cell wall-cuticle interface suggests an absence of esterified pectic HG (Figs. 7 and 8, right images).

Characterization of the cell wall-cuticle continuum of the *cyp77a6 dcr* double mutant showed that DCR is epistatic to CYP77a6 in terms of cuticle structure and organization. On the abaxial side of the petal, the cuticle proper contained dispersed HG-rich cell wall material, which was not true for the adaxial side (Figs. 7 and 8). The irregularities in thickness of the cuticle proper were more pronounced on the adaxial than the abaxial side of the petal, as in the *dcr* mutant (Figs. 7 and 8). The overall dimensions of the cell wall and cuticle were reduced, however, in comparison with the single mutants (Supplemental Fig. S8).

The cuticle of *dcr gpat6* showed features of both parental lines: the multiple layers of the *gpat6* cuticle and the irregularities of the *dcr* cuticle (Figs. 7 and 8). No

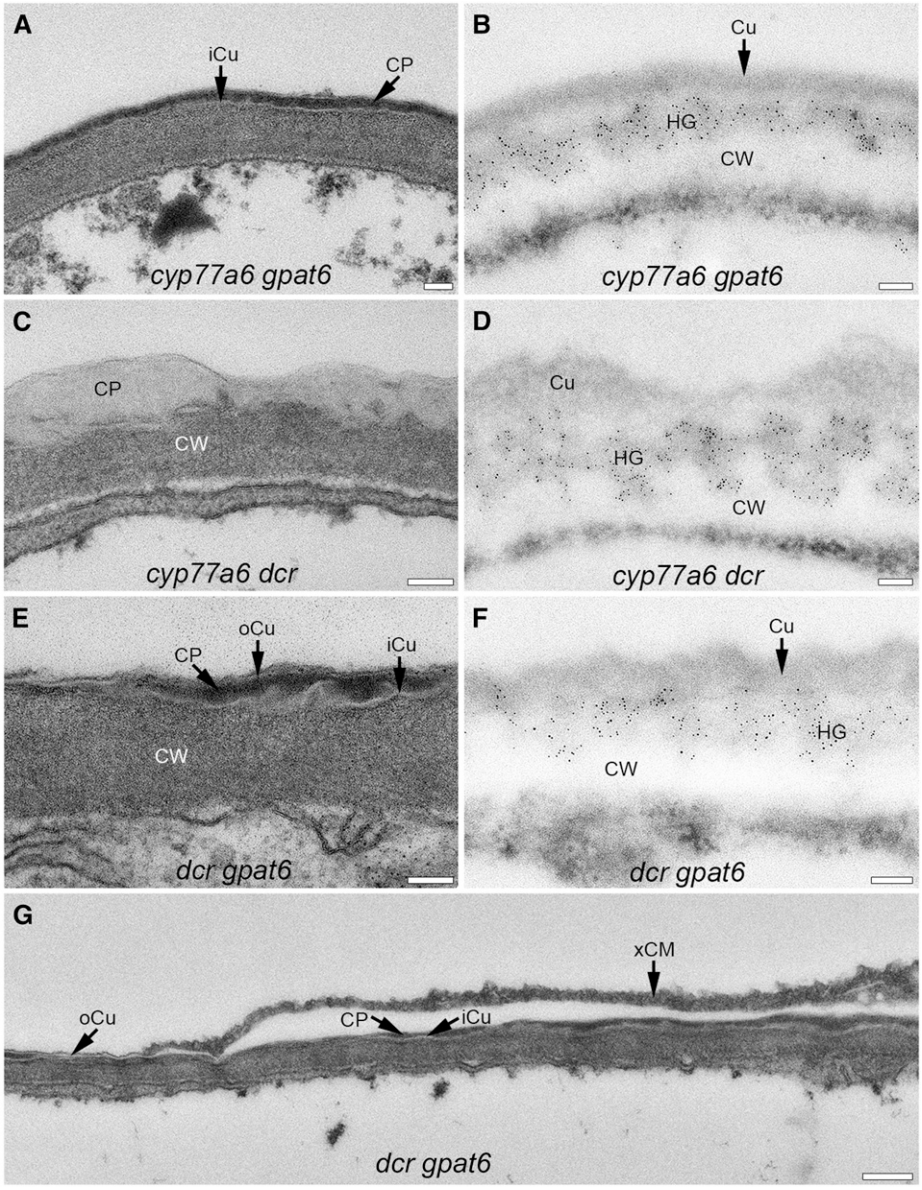

Figure 8. Ultrastructure of the cuticle and localization of HG in the cell wall-cuticle continuum in different double mutants having low amounts of 10,16-diOH C16:0. The cell wall-cuticle continuum on the adaxial side of the petal at the apex of epidermal cells is shown. The ultrastructure of the cuticle was depicted in A, C, E, and G on sections embedded in Spurr's resin. The LM20 labeling of esterified HG is depicted on LR White-embedded sections in B, D, and F. CP, Cuticle proper; Cu, cuticle; CW, cell wall, xCM, extracuticular material. Bars = 100 nm in A to F and 250 nm in G.

islands of material labeling with LM20 antibody occurred in the cuticle proper on the abaxial side of *dcr gpat6* petals, however (Figs. 7 and 8). The electron-opaque layer of the cuticle proper varied strongly in thickness in the double mutant, while the iCu and oCu layers remained unaltered in thickness (Figs. 7 and 8). Cell wall irregularities that occurred occasionally on the abaxial side of the cuticle of the *dcr gpat6* mutant could be interpreted as weak nanoridges, as in *gpat6*. In *dcr gpat6*, however, these structures were sometimes void of electron-opaque material, leaving only a scaffold of a partially multilayered cuticle (Fig. 7). A more extensive multilayered structure, potentially originating from two attempted nanoridges, disclosed again that electron-opaque layers alternate with electron-lucent ones (Fig. 7). The adaxial side of the *dcr gpat6* cuticle was, in general, more strongly altered and very irregular in thickness, as in *dcr*. Not only longer zones of a thin electron-opaque layer occurred, but occasionally also local depositions of electron-opaque material on the outside of the cuticle that remained connected to the extracellular matrix (Fig. 8). Whether this material is indeed lipidic in nature would need further investigation. Immunolabeling of *dcr gpat6* with LM20 confirmed the above-noted irregularities in thickness at the cell wall-cuticle interface but did not give indications of additional HG-rich material on the outer surface.

The above analyses of the cuticle ultrastructure of the double mutants *cyp77a6 dcr* and *dcr gpat6* support the notion that DCR is required for the organization of the cuticle proper independent of different compositions, having a particularly strong impact on the structure of the adaxial petal cuticle. The analyses reveal, moreover, that the absence of GPAT6 function

leading to a multilamellated cuticle is independent of the other observed cuticle modifications.

DISCUSSION

Cutin Monomers Are Connected in a Novel Fashion When 10,16-diOH C16:0 Is Absent

Qualitative features of the cell wall have been characterized in mutants of Arabidopsis and maize (*Zea mays*) using FTIR spectra (Chen et al., 1998; Mouille et al., 2003; McCann and Carpita, 2005). Attenuated total reflection FTIR spectroscopy also has been used to characterize the cuticle of different plant species, in particular those having a thick cuticle (Villena et al., 2000; Dokken et al., 2005). Petal blades are relatively thin, making them translucent to infrared radiation, allowing direct probing by transmission FTIR with almost no sample preparation (Mazurek et al., 2013). Here, the petals of Arabidopsis are characterized by transflection FTIR, since this method results in identical peak characteristics to the transmission mode but with an improved baseline. The intensity of the ν(C-H) and ν(C=O) vibrations correlated well with the total amounts of cutin monomers of the different genotypes, as shown previously (Mazurek et al., 2013; Fabre et al., 2016).

FTIR spectroscopy identified different types of petal cutin in different Arabidopsis genotypes based on the positions and morphology of the characteristic ν(C-H) and ν(C=O) band vibrations (Fig. 1). Enzymatic digestions contributed substantially to improving the determination of specific band vibrations in cutin and the subsequent classification of cutin mutants into three different spectrotypes (1, 2, and 3; Supplemental Fig. S3). Since the position of the band vibrations in FTIR spectroscopy gives information on the molecular structure in the vicinity of the chemical bond, the cutin monomer composition of the different genotypes suggested that the changes in the band vibrations in the ν(C-H) and ν(C=O) ranges of spectrotypes of 2 and 3 originated from the lack of midchain hydroxylated fatty acids that could form ester bonds. This conjecture was strengthened by the absence in 2 and 3 not only of the major wild-type ν(C=O) band at 1,732 cm^{-1} but also of the smaller of the two contributions at 2,926 and 2,856 cm^{-1} in the range of the ν_{asym}(C-H) and ν_{sym}(C-H) bands. The presence of two new ν(C=O) band vibrations in 2 and 3 at 1,732 and 1,746 cm^{-1} suggest that new types of ester linkages were formed whose infrared spectra intensities varied slightly, presumably dependent on the composition of the polyester. In the absence of 10,16-diOH C16:0, the remaining cutin monomers may be linked differently into a macromolecular structure by ester bonding among themselves. The incorporation of higher proportions of glycerol or other nonaliphatic molecules into cutin also might give rise to a polyester network generating new band vibrations (Philippe et al., 2016; Yang et al., 2016). However, it cannot be ruled out that the distinctions in the ν(C=O) band vibrations also might be due to differences in ester bond modifications of nonpectic polysaccharides, such as methylation or acetylation, or to polysaccharide-cutin interactions.

Cutin monomer analysis and genetics have strongly contributed to the interpretation of the FTIR spectra of Arabidopsis mutants. The molecular basis of the different contributions, however, will only be elucidated when refined methodologies have been established for analysis in vivo of cuticles containing minor amounts of polyester or similar changes are identified in cuticles suitable for biochemical characterization.

Some Facets of Petal Cuticle Ultrastructure Correlate to Cutin Spectrotypes

All genotypes having a wild-type-like cutin structure in FTIR spectroscopy, wild type, *lacs2*, and *pec1* (group 1), also manifested a cuticle proper that was directly and tightly attached to the underlying pectin-rich cuticular layer but forming a clearly distinct layer. This type of structural arrangement appears essential for the formation of nanoridges and requires the cutin monomer 10,16-diOH C16:0 or a precursor based on this fatty acid. Alterations and reductions in nanoridge formation in *pec1* and *lacs2* correlated well with the amounts of cutin present (Supplemental Fig. S4; Bessire et al., 2011; Fabre et al., 2016), since reductions in size and the number of nanoridges reduce the surface area covered with a cuticle proper. Changes in the density of the cuticle layer that had been observed in *pec1* were lacking in *lacs2*, indicating differences in the cell wall-cuticle continuum between these genotypes that could not be identified by FTIR spectroscopy (Bessire et al., 2011; Mazurek et al., 2013).

The *cyp77a6* and *dcr* mutants of group 2 have a very similar spectrotype and nearly identical cutin monomer composition and amount (Figs. 1 and 2; Supplemental Fig. S3). The *dcr* mutant may have these polyester characteristics due to an inhibitory mechanism acting on CYP77A6, potentially by a metabolite accumulating in the absence of DCR (Fig. 9). Several features of the ultrastructure of their cuticles also were very similar, such as the contrast of the cuticle proper, the presence of pectic HG in the cuticle proper, and the absence of nanoridges. The broad cuticle proper in relation to its polyester content may result from a loose polyester structure built exclusively of ω-oxygenated cutin monomers having a high proportion of unsaturated C16, which is less osmiophilic. Additional differences in the thickness of the cuticle proper in *dcr* were identified by studying its ultrastructure. These differences, however, were neither reflected by the FTIR spectrum nor by cutin monomer composition and will be discussed further below.

The small FTIR spectrum differences between the *gpat6* (group 3) and group 2 spectrotypes, manifested in the ratios of the contributions at 1,736 and 1,742 cm^{-1}, predicted relatively small changes in ultrastructure. Petals of *gpat6*, however, not only had a thinner and more contrasted cuticle proper, probably resulting from a higher proportion of osmiophilic unsaturated cutin

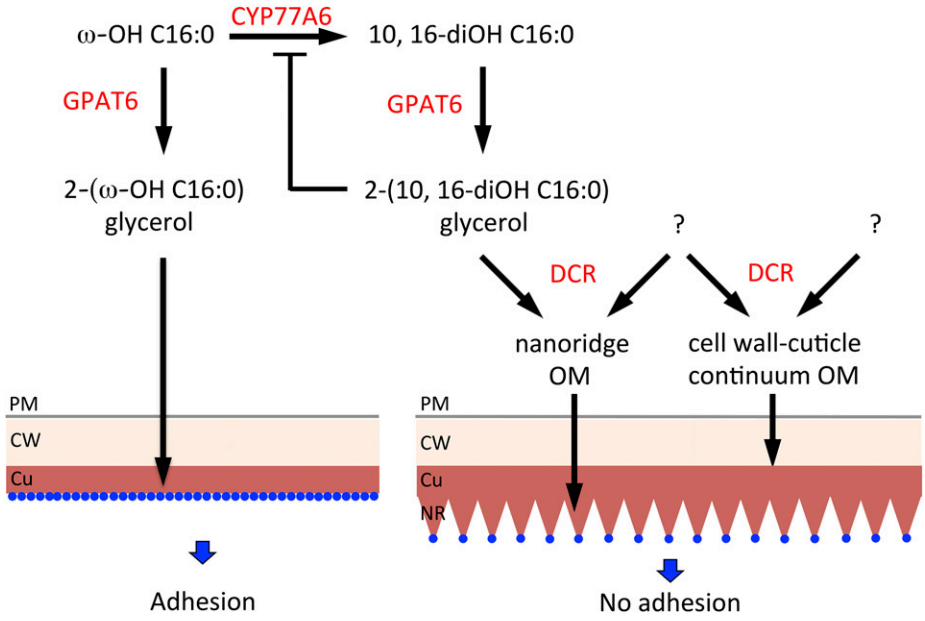

Figure 9. Model of the relationship between C16 cutin precursor synthesis and the ultrastructure and physical properties of the petal cuticle. Cutin biosynthetic enzymes (in red) determine the ultrastructure of the cell wall-cuticle continuum and the physical properties of the cuticle. CYP776A performs the midchain hydroxylation of *ω*-OH C16:0, giving 10,16-diOH C16:0 that is esterified to glycerol by GPAT6. The resulting monoacylglycerol is further metabolized by DCR to a molecule required for nanoridge formation, potentially by linking it to a nonaliphatic component (?). Independent of 10,16-diOH C16:0 as substrate, DCR forms with unknown substrates cell wall-cuticle organizing molecules. The nanoridges present on petals reduce interactions with other surfaces, leading to a cuticle lacking adhesion. In the absence of DCR, CYP77A6 is hypothesized to be inactive, and only *ω*-OH C16:0 is incorporated in the cuticle via a GPAT6-dependent pathway not involving DCR. Defects in DCR, CYP77A6, and GPAT6 result in a nanoridge-free petal surface having a high degree of interaction with other surfaces and undergoing adhesion. The necessary transport steps that are involved in the transfer of cutin precursors to the cuticle are not shown. Blue dots symbolize possible zones of interaction with other surfaces. Cu, Cuticle; CW, cell wall; NR, nanoridge; OM; organizing molecule, PM, plasma membrane.

monomers, but also had a differently structured cell wall-cuticle interface characterized by an additional electron-translucent lamella. Such an electron-translucent interface between the cell wall and cuticle has been observed previously in a cuticle rich in unsaturated C18 monomers (Fabre et al., 2016). This suggests that such a structure typically connects a cuticle rich in *ω*-oxygenated C18 monomers to the cell wall. Why such a remarkable difference in ultrastructure occurs when no differences in chemical linkages were revealed by FTIR is puzzling. The reason might be that differently linked *ω*-oxygenated cutin monomers have *ν*(C=O) vibrations at a similar wavelength.

Structuring the Cell Wall-Cuticle Continuum of Petal Epidermal Cells

Immunocytochemical studies have revealed the deposition of pectic HG underneath the cuticle proper in the fibrous structured outermost zone of the polysaccharide-rich cell wall. This was expected, since pectin has been found at the interface with the cuticle and has been exploited for years to isolate cuticles using pectinases (Orgell, 1955; Jeffree, 2006). The pectin-rich cell wall layer included also that within the nanoridges in the wild type and *lacs2*.

No pectic HG-rich cell wall material has been ascertained in the cuticle proper in the wild type and most other genotypes. The exception is on the abaxial side of the single and double group 2 mutants. This dispersed, fibrous cell wall material could be labeled with LM20, indicating the presence of esterified pectin and very likely other polysaccharides. The variation in the structure of the cell wall-cuticle continuum between the two sides of the petal might be caused by regulated differences in polysaccharide composition. That low amounts of HG and other polysaccharides are present in wild-type Arabidopsis that go undetected by structural TEM and immunolabeling may result, in part, from the polyester structure hindering accessibility by the antibody, for example by a higher degree of cutin cross-linking. To maximize the potential of HG detection in the cuticle, very small gold particles (4 nm) were used, resulting in very strong labeling in the cell wall. In contrast to tomato fruits containing pectin and cellulose (Segado et al., 2016), Arabidopsis petals may only have pectin-containing polysaccharides in the cuticle layer of the cell wall, where it potentially contributes to nanoridge formation. Its absence in the cuticle proper may

explain the amorphous appearance of the Arabidopsis petal cuticle.

A remarkable regulatory aspect has come to light concerning the potential coordinated deposition of cell wall (including the cuticle layer) and cuticle proper in the formation of nanoridges on the surface of petals. This is based on the observation that Arabidopsis mutants having a very thin cuticle proper also have a thinner cell wall, implying a type of feedback regulation between the formation of the cuticle and the cell wall leading to an equilibrated assembly of the entire cell wall-cuticle continuum. The impact of the reduction in thickness of the entire cell wall-cuticle continuum was assessed also during the adhesion and/or tearing experiments. The forces necessary to tear the tissue of a petal correlated well to the thickness of the entire cell wall of petals, which was greatest in *cyp77a6* and smallest in *gpat6*.

Complementary Functions of GPAT6 and DCR in the Formation of the Petal Cuticle

The knockout of the midchain hydroxylase CYP77A6 causes the lack of 10,16-diOH C16:0 in the cuticle and leads to the overaccumulation of the metabolic precursor ω-OH C16:0 (Fig. 9). These changes not only lead to the absence of nanoridges, as reported here and earlier (Li-Beisson et al., 2009; Panikashvili et al., 2009), but also play an important role in the organization of the cell wall-cuticle interface. The loose cuticle structure of the *cyp77a6* mutant having cell wall protrusions and polysaccharide islands within the cuticle proper can be attributed to a cutin rich in ω-oxygenated C16:0, since both the *gpat6* and *cyp77a6 gpat6* mutants, having strong reductions in all C16:0 monomers in cutin, have a well-delimitated cell wall (Fig. 9).

The analysis of the *dcr* cuticle ultrastructure revealed a high variation in thickness indicating a crucial function of DCR in cuticle organization, although other methods failed to differentiate the *dcr* and *cyp77a6* mutants. Double mutant analyses revealed that DCR was epistatic to CYP77A6 and additive to GPAT6. This demonstrates that 10,16-diOH C16:0 and/or the GPAT6 product mono(10,16-diOH C16:0)-2-glycerol absolutely requires DCR function for its incorporation into cutin (Fig. 9). The analysis of the petals of the *dcr gpat6* double mutants showed that DCR also is required for the organization of a cuticle rich in unsaturated C18 monomers, as in rosette leaves having a C18:2-rich cuticle (Panikashvili et al., 2009). The knockout of *DCR* expression in mutants having different aliphatic cutin monomer compositions led to several distinct alterations in the organization of the cell wall-cuticle continuum, including an irregular thickness of the cell wall-cuticle continuum, the formation of an altered cell wall-cuticle interface, and nanoridge formation. Thus, DCR can be hypothesized to form molecules that contribute to the organization of the cell wall-cuticle continuum. DCR-dependent precursors carrying 10,16-diOH C16:0 are essential for the formation of nanoridges (Fig. 9). In addition, DCR is hypothesized to generate currently unidentified precursors that are essential for organizing the cell wall-cuticle continuum (Fig. 9). The essential role of DCR in organizing the cell wall-cuticle continuum also has been seen in tomato fruits, where the down-regulation of *DCR* expression led to cuticle cracking, which in turn induced suberin formation in a wound-healing process (Lashbrooke et al., 2016). The mechanism by which the enzymatic activity of DCR is linked to cuticle and cell wall organization will need further investigations. In vitro DCR has diglycerolacyltransferase activity necessary for tri(10,16-diOH C16:0)-glycerol formation (Rani et al., 2010). Some of the observed phenotypes of *dcr gpat6*, however, such as the ectopic accumulation of cuticle material, also might be attributed to the strong developmental abnormalities, including organ fusions. These most likely cause the up-regulation of cutin biosynthesis genes, as in *bodyguard* (*bdg*) and *fiddlehead* (*fdh*), of Arabidopsis (Kurdyukov et al., 2006; Voisin et al., 2009).

The loss of GPAT6 function in Arabidopsis results in changes in the cuticle layers but not in their organization within the petal cuticle. The petal cuticles of the *gpat6* mutant and *dcr gpat6* double mutant are examples of those built from polyesters rich in unsaturated C18 monomers. The electron-opaque material is sandwiched between two electron-translucent layers that did not change in thickness. This argues that the electron-translucent lamellae represent a scaffold, potentially of nonlipid nature. This type of sandwich organization of electron-translucent and electron-opaque layers may be interpreted as the beginning of the formation of the lamellated cuticle that exists in many species but that is normally not formed in Arabidopsis (Jeffree, 2006). The formation of electron-translucent lamella also may be related to the formation of suberin lamellae that are rich in unsaturated C18 monomers. An explanation for the regular alternation of electron-translucent lamellae and electron-opaque lamellae has been sought a long time and is still elusive, as discussed (Nawrath et al., 2013; Vishwanath et al., 2015). Thus, knocking out the expression of *GPAT6* in Arabidopsis had a different effect on cuticle structure in petals compared with a similar *GPAT6* knockout in tomato, where the fruits showed a reduction in cutin amount and cuticle thickness but maintained a similar composition and molecular structure compared with the wild type (Philippe et al., 2016; Petit et al., 2016).

Nanoridges Decrease Contact Forces to Other Surfaces, Supporting Petal Outgrowth

This study shows that nanoridges and conical cells diminish the contact surface between solid phases and reduce their interaction, potentially by van der Waals forces, or physical adhesion (Figs. 4 and 9; Supplemental Figs. S5 and S6). Petals undergo a fast outgrowth from

the floral bud, during which the petal has to pass other organs. Physical adhesion between floral organs would strongly impact floral development. Thus, nanoridge formation might have been under positive selective pressure to decrease solid-state adhesion. Several Arabidopsis mutants have been isolated recently having folded petals that are unable to emerge from the floral bud (Takeda et al., 2013, 2014). FOLDED PETAL1 encodes the bifunctional wax ester synthase/diacylglycerol acyltransferase WSD11 that was hypothesized to alter adhesion properties in young outgrowing petals before nanoridges form by generating a lubricant (Takeda et al., 2013). *FOLDED PETAL2* was allelic to *ABCG13*, encoding an ABCG transporter involved in cutin deposition in flowers (Panikashvili et al., 2011; Takeda et al., 2014), supporting our hypothesis that nanoridge formation and, in part, also conical cell shape might be of biological relevance during the fast elongation of petals by reducing adhesion to other plant surfaces.

Thus, the physical adhesion is of a very different nature than molecular cell-to-cell adhesions occurring during early development between organs having permeable cuticles, including petals of *gpat6* and *dcr*, that are typically called organ fusions (Nawrath et al., 2013) and cell-to-cell adhesions based on pectin or pectin-dependent signaling (Wolf et al., 2009; Verger et al., 2016). A petal cuticle is consequentially involved in several adhesion processes modifying the development of the floral organs. The folding of petals is a relatively late process based on weak adhesion processes occurring during petal outgrowth. During this study, petal folding occurred in *dcr* and occasionally also in *lacs2* and *cyp77a6*. Organ fusion is a very early developmental process causing strong floral abnormalities, potentially including reduction of petal number. This was observed in *gpat6*, as described previously (Fabre et al., 2016), and was even stronger in *gpat6* double mutants with *cyp77a6* and *dcr* generated during this study.

CONCLUSION

The characterization of different genotypes of Arabidopsis with alterations in petal cutin formation revealed that 10,16-diOH C16:0 plays a central role in the formation of the petal cuticle and has a profound impact on the molecular structure of cutin and the ultrastructure of the cuticle, directly influencing the nanostructure of the cuticle surface and its physical properties in Arabidopsis (Fig. 9). This study also highlights some of the gaps in our understanding of cuticle formation, including the three-dimensional structure of cutin and the organization of the cell wall-cuticle continuum, which is influenced by DCR (Fig. 9).

The physical and chemical properties of the petal surface of cutin mutants of Arabidopsis pointed to a crucial role of cutin in the generation of specialized plant surfaces with important biological functions, such as the gliding of organs during rapid growth (Takeda et al., 2013, 2014). The presence of polysaccharide cell wall material in the cuticle proper may contribute to the particular function of a specific cuticle. For example, cellulose and pectin in the cuticle of tomato fruits might give mechanical strength to the cuticle and thus exert its protective function (Segado et al., 2016). Cuticles forming on particular surface structures, such as the nanoridges of petals, likely have different compositional and structural features that still remain to be determined.

MATERIALS AND METHODS

Plant Material and Growth Conditions

Arabidopsis (*Arabidopsis thaliana*) accession Columbia-0 and the following mutant alleles were used during this study: *lacs2-3* (T-DNA insertion in gene At1g49430; Bessire et al., 2007), *pec1-2* and *pec1-3* (T-DNA insertions in gene At2g26910; Bessire et al., 2011; Fabre et al., 2016), *cyp77a6-1* and *cyp77a6-2* (T-DNA insertions in gene At3g10570; Li-Beisson et al., 2009), *gpat6-2* (T-DNA insertion in gene At2g38110; Li-Beisson et al., 2009; Fabre et al., 2016), and *dcr-2* (T-DNA insertion in gene At5g23940; Panikashvili et al., 2009). *gpat6-2* and *cyp77a6* mutant alleles were obtained from Frédéric Beisson (Commissariat à l'Energie Atomique-Centre National de la Recherche Scientifique-Aix Marseille Université), and *dcr-2* was obtained from Asaph Aharoni (Weizmann Institute). Since no spectroscopic differences were identified between *pec1-2* and *pec1-3* (Fabre et al., 2016) and *cyp77a6-1* and *cyp77a6-2*, allele designations were omitted.

The *cyp77a6-1 gpat6-2*, *cyp77a6-1 dcr*, and *dcr gpat6-2* double mutants were identified by a combination of Toluidine Blue staining of leaves and genotyping of the F2 population of the respective genetic crosses.

Plants were grown under long-day conditions in a light/dark cycle of 16/8 h at 20°C under 100 μmol m^{-2} s^{-1} warm white light (color 830) and 65% humidity. Short-day plants were grown for 10 h at 20°C and 65% humidity under 100 μmol m^{-2} s^{-1} warm white light and for 14 h at 17°C and 80% humidity in the dark.

Preparation of Plant Tissues for FTIR Spectroscopy

Fully open flowers (at anthesis and anthesis plus 1 d) were extracted with 6 mL of methanol for at least 20 h with two solvent changes. Entire flowers were placed on a golden plate for FTIR microspectroscopy in transflection mode in such a way that petals were fully expanded.

Leaf epidermis was prepared from fully expanded rosette leaves of 5-week-old short-day-grown plants using the blender method described by Geiger et al. (2011). Tissue fragments were treated with several changes of methanol, and fragments of epidermal pavement cells were selected for analysis using the FTIR microscope.

Enzymatic and chemical treatments of petals were performed as described previously (Mazurek et al., 2013). For double digestions, entire methanol-extracted flowers were incubated with several changes of the respective digestion buffer to equilibrate tissues and then digested as described, except that the incubation time with pectolyase was reduced to 2 to 3 h for *cyp77a6*, *dcr*, and *gpat6*. Digested flowers were carefully transferred to methanol that was replaced several times before FTIR analysis.

FTIR Spectroscopy

FTIR spectroscopy measurements were performed as described previously (Mazurek et al., 2013) using a transflection mode; that is, plant material was located on a golden slide and a laser beam was passed through the entire sample twice due to reflection by the gold. The use of transflection resulted in the improvement of the signal quality if compared with data collected in transmission mode and eliminated a sinusoidal baseline distortion associated with the use of KBr discs. Spectra were recorded at the resolution of 4 cm^{-1}, applying a zero filling factor of 2, and recording 96 scans per sample. Afterward, they were baseline corrected and normalized by dividing by the area under curves. The second derivative of spectra was computed using the Savitski-Golay function (11 points and third degree polynomial). Infrared studies were performed utilizing plant material from five sets of independently grown plants. Spectra were recorded for six petals of six different flowers harvested from six different plants, so the resulting spectrotype for each genotype was determined as an average of about 150 FTIR measurements. After

treatment of petals, average spectra were computed from at least 10 spectra of five to six different petals.

Chemical Analysis

For the chemical analysis of floral polyesters, 30 entire flowers from four to six plants were pooled. For the analysis of petal blades, petal blades from 800 to 1,000 flowers of 12 plants were pooled. Four to six replicates were made from each type. The polyester composition was analyzed after transesterification by base catalysis and following acetylation as described previously (Barberon et al., 2016).

Electron Microscopy Techniques

Cryoscanning electron microscopy was performed as described previously (Mazurek et al., 2013). For the analysis of the cuticle-cell wall structure, petals were prepared for TEM by embedding in Spurr's resin as described previously (Fabre et al., 2016).

For the characterization of the distribution of pectin in the cell wall, plant samples were embedded in LR White resin as follows. Entire flowers were fixed in 1.5% glutaraldehyde solution (EMS) and 2% formaldehyde (EMS) in phosphate buffer (0.1 M, pH 7.4; Sigma) for 2 h at room temperature. The samples were then washed two times in distilled water and dehydrated in ethanol (Sigma) at graded concentrations (30%, 40 min; 50%, 40 min; 70%, 40 min; and 100%, three times, 1 h). This procedure was followed by infiltration in LR White resin (Sigma) at graded concentrations (LR White 1:3 ethanol, 12 h; LR White 3:1 acetone, 12 h; LR White 1:1, two times, 8 h). The Arabidopsis flowers were then dissected in the resin using a dissecting microscope. Petals were placed in molds filled with resin and then polymerized for 48 h at 60°C in an oven in a nitrogen environment. Ultrathin sections (60 nm) were cut on a Leica Ultracut (Leica Microsystems) and picked up on a copper-slot grid (2 × 1 mm; EMS) coated with a polystyrene film (Sigma).

For immunogold labeling, LM19 and LM20 (IgM) rat monoclonal antibodies were used (PlantProbes). Ultrathin sections were first incubated in 50 mM ammonium chloride (Sigma) solution for 1 h in order to block aldehydes. Then, sections were treated with 1% acetylated bovine serum albumin solution (BSAc; Aurion) in potassium phosphate-buffered saline (PBS; 0.15 M, pH 7.4; Sigma) for 1 h to inhibit nonspecific binding of antibodies. Afterward, sections were incubated with the primary antibody, diluted 1:20 in 0.1% BSAc in PBS for 1 h at room temperature, washed six times in 0.1% BSAc in in PBS, and then incubated with the secondary antibody (4-nm Colloidal Gold-AffiniPure Goat Anti-Rat IgM; Jackson ImmunoResearch; our own measurements revealed that the gold grains varied between 2 and 6 nm in diameter), and diluted 1:50 in 0.1% BSAc in PBS for 1 h at room temperature. The sections were then washed four times in 0.1% BSAc in PBS, followed by four washing steps in PBS, fixed in 1% glutaraldehyde solution (EMS) in PBS for 5 min, washed 10 times in water, and finally stained with 2% uranyl acetate (Sigma) in water for 10 min and then rinsed several times with water. In parallel, some controls without primary or without secondary antibody were done (Supplemental Fig. S9). Alternatively, sections in Spurr's resin were immunogold labeled with the same protocol.

A control of the size of the gold particles also was done to be sure that the variety of sizes was not due to uranyl or other precipitates. A drop of secondary antibody (4-nm Colloidal Gold-AffiniPure Goat Anti-Rat IgM; Jackson ImmunoResearch), diluted 1:2 in PBS, was put on a copper-slot grid (2 × 1 mm; EMS) coated with a polystyrene film (Sigma) for 2 min, then rapidly washed in water, and dried. Transmission electron micrographs were taken with a Philips CM100 transmission electron microscope (FEI) at an acceleration voltage of 80 kV with a TemCam-F416 digital camera (TVIPS).

Petal Adhesion and Breakage Measurements

Fully open (at anthesis and anthesis plus 1 d) *cyp77a6*, *pec1-3*, *gpat6-2*, *lac2-3*, *dcr*, and Columbia-0 wild-type flowers were treated with methanol as described for FTIR spectroscopy. Individual flowers were removed from the methanol, and the flower was mounted on a precleaned microscope slide (Thermo Fisher) such that one petal blade adhered to the glass. The flowers were left to dry for 2 to 3 min prior to measuring. The force required to disrupt the contact between the microscope slide and the petal was quantified in gram equivalents using a load transducer, as described by Stenvik et al. (2008). A micro clamp connected to the transducer was attached to the receptacle of the flower prior to measuring. Depending on the genotype, it was either possible to measure the force required to detach the entire flower, including an undamaged petal, from the glass slide or the force needed to remove the flower by tearing the petal, leaving part of the petal attached to the slide. For some genotypes, the entire flower fell off when applying the clamp to the receptacle. The minimum force that could be measured was 0.5-g equivalents, which was thus the threshold of the experiment. A minimum of 30 petals was measured for each genotype.

Supplemental Data

The following supplemental materials are available.

Supplemental Figure S1. Spectral features of petals of different Arabidopsis genotypes before and after acid depolymerization.

Supplemental Figure S2. Classification of Arabidopsis cutin mutants by spectrotype.

Supplemental Figure S3. Spectral features of petals of different genotypes treated with proteinase K and pectolyase.

Supplemental Figure S4. Cutin monomer of petals of *lacs2* and *cyp77a6 gpat6* in comparison with respective controls.

Supplemental Figure S5. Shape and surface structure of epidermal cells on the adaxial side of the petal of Arabidopsis genotypes having a strongly reduced amount of 10,16-diOH C16:0.

Supplemental Figure S6. Shape and surface structure of epidermal cells on the adaxial side of the petal of Arabidopsis genotypes having reduced amounts of cutin.

Supplemental Figure S7. Cuticle ultrastructure on the abaxial side of petals in different genotypes of Arabidopsis.

Supplemental Figure S8. Dimensions of the plant extracellular matrix of petal epidermal cells in different Arabidopsis genotypes.

Supplemental Figure S9. Localization of HG in the cell wall-cuticle continuum on the adaxial side of petals of different Arabidopsis genotypes.

Supplemental Figure S10. Immunogold-labeling controls for epidermal petal cells of the Arabidopsis wild type.

ACKNOWLEDGMENTS

We thank Guillaume Gremion, Delphine Le Roux, and Sylvain Escande for technical assistance and Alice Berhin for contributions to maintaining the seed stocks; Frédéric Beisson for supplying seeds of the *cyp77a6* and *gpat6* mutants and Asaph Aharoni for seeds of *dcr*; Willy Blanchard for help in the preparation of the electron microscopy artwork; the reviewers and Penny von Wettstein-Knowles for critical comments; and Sebastian Poirier for contributions to the graphical design.

Received October 21, 2016; accepted December 13, 2016; published December 19, 2016.

LITERATURE CITED

Bak S, Beisson F, Bishop G, Hamberger B, Höfer R, Paquette S, Werck-Reichhart D (2011) Cytochromes p450. The Arabidopsis Book **9:** e0144, doi/10.1199/tab.0144

Baker MJ, Trevisan J, Bassan P, Bhargava R, Butler HJ, Dorling KM, Fielden PR, Fogarty SW, Fullwood NJ, Heys KA, et al (2014) Using Fourier transform IR spectroscopy to analyze biological materials. Nat Protoc **9:** 1771–1791

Barberon M, Vermeer JEM, De Bellis D, Wang P, Naseer S, Andersen TG, Humbel BM, Nawrath C, Takano J, Salt DE, et al (2016) Adaptation of root function by nutrient-induced plasticity of endodermal differentiation. Cell **164:** 447–459

Bargel H, Koch K, Cerman Z, Neinhuis C (2006) Structure-function relationships of the plant cuticle and cuticular waxes: a smart material? Funct Plant Biol **33:** 893–910

Beisson F, Li-Beisson Y, Pollard M (2012) Solving the puzzles of cutin and suberin polymer biosynthesis. Curr Opin Plant Biol **15:** 329–337

Bessire M, Borel S, Fabre G, Carraça L, Efremova N, Yephremov A, Cao Y, Jetter R, Jacquat AC, Métraux JP, et al (2011) A member of the

PLEIOTROPIC DRUG RESISTANCE family of ATP binding cassette transporters is required for the formation of a functional cuticle in *Arabidopsis*. Plant Cell **23:** 1958–1970

Bessire M, Chassot C, Jacquat AC, Humphry M, Borel S, Petétot JMC, Métraux JP, Nawrath C (2007) A permeable cuticle in Arabidopsis leads to a strong resistance to Botrytis cinerea. EMBO J **26:** 2158–2168

Bird D, Beisson F, Brigham A, Shin J, Greer S, Jetter R, Kunst L, Wu X, Yephremov A, Samuels L (2007) Characterization of Arabidopsis ABCG11/WBC11, an ATP binding cassette (ABC) transporter that is required for cuticular lipid secretion. Plant J **52:** 485–498

Chen L, Carpita NC, Reiter WD, Wilson RH, Jeffries C, McCann MC (1998) A rapid method to screen for cell-wall mutants using discriminant analysis of Fourier transform infrared spectra. Plant J **16:** 385–392

Dokken KM, Davis LC, Marinkovic NS (2005) Use of infrared microspectroscopy in plant growth and development. Appl Spectrosc Rev **40:** 301–326

España L, Heredia-Guerrero JA, Segado P, Benítez JJ, Heredia A, Domínguez E (2014) Biomechanical properties of the tomato (*Solanum lycopersicum*) fruit cuticle during development are modulated by changes in the relative amounts of its components. New Phytol **202:** 790–802

Fabre G, Garroum I, Mazurek S, Daraspe J, Mucciolo A, Sankar M, Humbel BM, Nawrath C (2016) The ABCG transporter PEC1/ABCG32 is required for the formation of the developing leaf cuticle in Arabidopsis. New Phytol **209:** 192–201

Fich EA, Segerson NA, Rose JKC (2016) The plant polyester cutin: biosynthesis, structure, and biological roles. Annu Rev Plant Biol **67:** 207–233

Geiger D, Maierhofer T, Al-Rasheid KAS, Scherzer S, Mumm P, Liese A, Ache P, Wellmann C, Marten I, Grill E, et al (2011) Stomatal closure by fast abscisic acid signaling is mediated by the guard cell anion channel SLAH3 and the receptor RCAR1. Sci Signal **4:** ra32

Guzman-Puyol S, Benítez JJ, Domínguez E, Bayer IS, Cingolani R, Athanassiou A, Heredia A, Heredia-Guerrero JA (2015) Pectin-lipid self-assembly: influence on the formation of polyhydroxy fatty acids nanoparticles. PLoS ONE **10:** e0124639

Hayat MA (2000) Principles and Techniques of Electron Microscopy: Biological Applications. Cambridge University Press, Cambridge, UK

Heredia A (2003) Biophysical and biochemical characteristics of cutin, a plant barrier biopolymer. Biochim Biophys Acta **1620:** 1–7

Heredia-Guerrero JA, Benítez JJ, Domínguez E, Bayer IS, Cingolani R, Athanassiou A, Heredia A (2014) Infrared and Raman spectroscopic features of plant cuticles: a review. Front Plant Sci **5:** 305

Heredia-Guerrero JA, Benitez JJ, Heredia A (2008) Self-assembled polyhydroxy fatty acid vesicles: a mechanism for plant cutin synthesis. BioEssays **30:** 273–277

Heredia-Guerrero JA, de Lara R, Domínguez E, Heredia A, Benavente J, Benítez JJ (2012) Chemical-physical characterization of isolated plant cuticles subjected to low-dose γ-irradiation. Chem Phys Lipids **165:** 803–808

Jeffree CE (2006) The fine structure of the plant cuticle. *In* M Riederer, C Müller, eds, Biology of the Plant Cuticle. Blackwell Publishing, Oxford, pp 11–125

Kolattukudy PE (2001) Cutin from plants. Biopolymers Online **3:** 1–35

Kretzschmar T, Burla B, Lee Y, Martinoia E, Nagy R (2011) Functions of ABC transporters in plants. Essays Biochem **50:** 145–160

Kurdyukov S, Faust A, Nawrath C, Bär S, Voisin D, Franke R, Schreiber L, Saedler H, Métraux J-P, Yephremov A (2006) The epidermis-specific extracellular BODYGUARD controls cuticle development and morphogenesis in Arabidopsis. Plant Cell **18:** 321–339

Lashbrooke JG, Cohen H, Levy-Samocha D, Tzfadia O, Panizel I, Zeisler V, Massalha H, Stern A, Trainotti L, Schreiber L, et al (2016) MYB107 and MYB9 homologs regulate suberin deposition in angiosperms. Plant Cell **28:** 2097–2116

Li-Beisson Y, Pollard M, Sauveplane V, Pinot F, Ohlrogge J, Beisson F (2009) Nanoridges that characterize the surface morphology of flowers require the synthesis of cutin polyester. Proc Natl Acad Sci USA **106:** 22008–22013

Li-Beisson Y, Shorrosh B, Beisson F, Andersson MX, Arondel V, Bates PD, Baud S, Bird D, Debono A, Durrett TP, et al (2013) Acyl-lipid metabolism. The Arabidopsis Book **11:** e0161, doi/10.1199/tab.0161

López-Casado G, Matas AJ, Domínguez E, Cuartero J, Heredia A (2007) Biomechanics of isolated tomato (*Solanum lycopersicum* L.) fruit cuticles: the role of the cutin matrix and polysaccharides. J Exp Bot **58:** 3875–3883

Luo B, Xue XY, Hu WL, Wang LJ, Chen XY (2007) An ABC transporter gene of *Arabidopsis thaliana*, AtWBC11, is involved in cuticle development and prevention of organ fusion. Plant Cell Physiol **48:** 1790–1802

Mazurek S, Mucciolo A, Humbel BM, Nawrath C (2013) Transmission Fourier transform infrared microspectroscopy allows simultaneous assessment of cutin and cell-wall polysaccharides of Arabidopsis petals. Plant J **74:** 880–891

McCann MC, Carpita NC (2005) Looking for invisible phenotypes in cell wall mutants of Arabidopsis thaliana. Plant Biosyst **139:** 80–83

Mouille G, Robin S, Lecomte M, Pagant S, Höfte H (2003) Classification and identification of Arabidopsis cell wall mutants using Fourier-transform infrared (FT-IR) microspectroscopy. Plant J **35:** 393–404

Nawrath C (2006) Unraveling the complex network of cuticular structure and function. Curr Opin Plant Biol **9:** 281–287

Nawrath C, Schreiber L, Franke RB, Geldner N, Reina-Pinto JJ, Kunst L (2013) Apoplastic diffusion barriers in Arabidopsis. The Arabidopsis Book **11:** e0167, doi/10.1199/tab.0167

Orgell WH (1955) The isolation of plant cuticle with pectic enzymes. Plant Physiol **30:** 78–80

Panikashvili D, Shi JX, Bocobza S, Franke RB, Schreiber L, Aharoni A (2010) The Arabidopsis DSO/ABCG11 transporter affects cutin metabolism in reproductive organs and suberin in roots. Mol Plant **3:** 563–575

Panikashvili D, Shi JX, Schreiber L, Aharoni A (2009) The Arabidopsis DCR encoding a soluble BAHD acyltransferase is required for cutin polyester formation and seed hydration properties. Plant Physiol **151:** 1773–1789

Panikashvili D, Shi JX, Schreiber L, Aharoni A (2011) The Arabidopsis ABCG13 transporter is required for flower cuticle secretion and patterning of the petal epidermis. New Phytol **190:** 113–124

Petit J, Bres C, Mauxion JP, Tai FW, Martin LB, Fich EA, Joubès J, Rose JK, Domergue F, Rothan C (2016) The glycerol-3-phosphate acyltransferase GPAT6 from tomato plays a central role in fruit cutin biosynthesis. Plant Physiol **171:** 894–913

Philippe G, Gaillard C, Petit J, Geneix N, Dalgalarrondo M, Bres C, Mauxion JP, Franke R, Rothan C, Schreiber L, et al (2016) Ester cross-link profiling of the cutin polymer of wild-type and cutin synthase tomato mutants highlights different mechanisms of polymerization. Plant Physiol **170:** 807–820

Rani SH, Krishna THA, Saha S, Negi AS, Rajasekharan R (2010) Defective in cuticular ridges (DCR) of *Arabidopsis thaliana*, a gene associated with surface cutin formation, encodes a soluble diacylglycerol acyltransferase. J Biol Chem **285:** 38337–38347

Segado P, Domínguez E, Heredia A (2016) Ultrastructure of the epidermal cell wall and cuticle of tomato fruit (*Solanum lycopersicum* L.) during development. Plant Physiol **170:** 935–946

Shi JX, Malitsky S, De Oliveira S, Branigan C, Franke RB, Schreiber L, Aharoni A (2011) SHINE transcription factors act redundantly to pattern the archetypal surface of Arabidopsis flower organs. PLoS Genet **7:** e1001388

Stenvik GE, Tandstad NM, Guo Y, Shi CL, Kristiansen W, Holmgren A, Clark SE, Aalen RB, Butenko MA (2008) The EPIP peptide of INFLORESCENCE DEFICIENT IN ABSCISSION is sufficient to induce abscission in *Arabidopsis* through the receptor-like kinases HAESA and HAESA-LIKE2. Plant Cell **20:** 1805–1817

Takeda S, Iwasaki A, Matsumoto N, Uemura T, Tatematsu K, Okada K (2013) Physical interaction of floral organs controls petal morphogenesis in Arabidopsis. Plant Physiol **161:** 1242–1250

Takeda S, Iwasaki A, Tatematsu K, Okada K (2014) The half-size ABC transporter FOLDED PETALS 2/ABCG13 is involved in petal elongation through narrow spaces in *Arabidopsis thaliana* floral buds. Plants (Basel) **3:** 348–358

Verger S, Chabout S, Gineau E, Mouille G (2016) Cell adhesion in plants is under the control of putative O-fucosyltransferases. Development **143:** 2536–2540

Verhertbruggen Y, Marcus SE, Haeger A, Ordaz-Ortiz JJ, Knox JP (2009) An extended set of monoclonal antibodies to pectic homogalacturonan. Carbohydr Res **344:** 1858–1862

Villena JF, Dominguez E, Heredia A (2000) Monitoring biopolyesters present in plant cuticles by FT-IR spectroscopy. J Plant Physiol **156:** 419–422

Vishwanath SJ, Delude C, Domergue F, Rowland O (2015) Suberin: biosynthesis, regulation, and polymer assembly of a protective extracellular barrier. Plant Cell Rep **34:** 573–586

Voisin D, Nawrath C, Kurdyukov S, Franke RB, Reina-Pinto JJ, Efremova N, Will I, Schreiber L, Yephremov A (2009) Dissection of the complex phenotype in cuticular mutants of Arabidopsis reveals a role of SERRATE as a mediator. PLoS Genet **5:** e1000703

Wolf S, Mouille G, Pelloux J (2009) Homogalacturonan methyl-esterification and plant development. Mol Plant **2:** 851–860

Yang W, Pollard M, Li-Beisson Y, Beisson F, Feig M, Ohlrogge J (2010) A distinct type of glycerol-3-phosphate acyltransferase with sn-2 preference and phosphatase activity producing 2-monoacylglycerol. Proc Natl Acad Sci USA **107:** 12040–12045

Yang W, Pollard M, Li-Beisson Y, Ohlrogge J (2016) Quantitative analysis of glycerol in dicarboxylic acid-rich cutins provides insights into Arabidopsis cutin structure. Phytochemistry **130:** 159–169

Yang W, Simpson JP, Li-Beisson Y, Beisson F, Pollard M, Ohlrogge JB (2012) A land-plant-specific glycerol-3-phosphate acyltransferase family in Arabidopsis: substrate specificity, sn-2 preference, and evolution. Plant Physiol **160:** 638–652

Yeats TH, Martin LBB, Viart HMF, Isaacson T, He Y, Zhao L, Matas AJ, Buda GJ, Domozych DS, Clausen MH, et al (2012) The identification of cutin synthase: formation of the plant polyester cutin. Nat Chem Biol **8:** 609–611

Yeats TH, Rose JKC (2013) The formation and function of plant cuticles. Plant Physiol **163:** 5–20